Cooperative Control for Multirotors Transporting an Unknown Suspended Load under Environmental Disturbances

Kristian Klausen, *Member, IEEE,* Chris Meissen, *Member, IEEE,* Thor I. Fossen, *Fellow, IEEE,* Murat Arcak, *Fellow, IEEE,* and Tor Arne Johansen, *Senior Member, IEEE*

***Abstract*—In this article, we develop a cooperative control algorithm for a group of multirotor Unmanned Aerial Vehicles (UAVs) transporting a suspended payload of unknown mass. In addition, the vehicles are subjected to unknown environmental disturbances in the form of wind. The control structure is analyzed using Lyapunov theory, and both numerical simulations and results from experimental field trials on an outdoor multirotor platform further validate the proposed control algorithm.**

***Index Terms*—Unmanned Aerial Vehicles, Cooperative Control, Passivity-based Control**

I. Introduction

THE multirotor is a highly versatile type of UAV, that has been the subject of research for many different applications. In addition to the standard applications to remote sensing and photography, transportation of objects through a suspended wire has lately received attention in the literature [1], [2]. A multirotor with the ability to transport a suspended load can be used for geomatic surveying, in-situ water sampling [3], mine detection [4], advanced Fixed-Wing UAV recovery systems [5] and package delivery. The latter has received commercial attention as well [6]–[8].

Using several multirotors can lead to an increased carrying capacity, and greater control of the suspended payload. When three or more multirotors lift the same payload, the suspended load is prohibited from swinging during acceleration. This has previously been studied in [1], [9]–[16].

In [1], [9], autonomous helicopter UAVs were used to transport a camera in a simulated search and rescue operation, and field trials were conducted. Manipulation of both the position and attitude of a suspended payload is considered in [10], [11], which also include results from indoor experiments using fast external camera systems for positioning. Geometric control is utilized in [12], [13], where the latter also includes preliminary experimental results conducted in the lab. An approach utilizing synchronization along a parameterized path is considered in [14]. In [15], model-predictive control is applied to a group of multirotors, where the controller also considers obstacle and collision avoidance and the results are verified with numerical simulations.

This article is an extension of the work in [16], [17]. In [17] a general passivity-based framework for cooperative control is presented. In [16] this framework is adapted to the case of multiple UAVs carrying a suspended load. It is shown that under the resulting control strategy the system is locally stable about a continuum of equilibrium points.

The main contributions of this article are the development of a control strategy combining elements of [16], [17] and the experimental verification of this strategy in a real-world scenario without relying on external local sensing systems. The control strategy developed extends the work in [17] to account for the physical interaction between subsystems via the suspended load. Compared to [16], this approach includes the effect of environmental disturbances and a simplified load model which allows us to prove global asymptotic stability of the system. This strategy was experimentally verified using commercially available autopilots and low-cost GNSS RTK systems. In the experiment three multirotors each weighing 2.3 kg lift a suspended load of approx. 2.2 kg cooperatively. Similar outdoor experiments where performed in [1], [9], but used a master-slave architecture instead of a synchronization approach for cooperative control. This approach is advantageous because all the UAVs are working cooperatively to achieve the same goal, instead of following the lead UAV. It is also simpler because the implementation is the same on each UAV.

A. Organization

This article is organized as follows. The system configuration and dynamics are introduced in Section II, which also includes modeling of the interconnected slung load system using the Udwadia-Kalaba equation for simulation purposes. Next, in Section III, a passivity-based control strategy is utilized to synthesize a position-based control law for the coordination of the UAVs. A simulation study is presented in Section IV, followed by experimental validation on a team of three multirotors in Section V.

K. Klausen, T. I. Fossen and T. A. Johansen are with the Department of Engineering Cybernetics, Norwegian University of Science and Technology, 7491 Trondheim, Norway (e-mail: kristian.klausen@ntnu.no, thor.fossen@ntnu.no, thor.arne.johansen@ntnu.no).

C. Meissen is with the Department of Mechanical Engineering at the University of California, Berkeley, CA, USA (e-mail: cmeissen@berkeley.edu)

M. Arcak is with the Department of Electrical Engineering and Computer Sciences at the University of California, Berkeley, CA, USA (e-mail: arcak@berkeley.edu)

This work was partially supported by the Research Council of Norway through its Centers of Excellence funding scheme, grant number 223254 (NTNU Centre for Autonomous Marine Operations and Systems), and by the National Science Foundation of the U.S., grant number ECCS-1405413

Manuscript submitted June, 2017; revised –

Fig. 1. Image of the experiment. From left to right, we see multirotors 1, 3 and 2. The wind was blowing heavily from right to the left, so it is apparent that more force from the suspended load is applied to the rightmost multirotor.

II. System Dynamics

The dynamics of a single multirotor UAV is well studied in the literature; see for instance [18] and references therein. A multirotor UAV is a rigid body with control actuation in all three rotational directions, as well as upwards thrust in the positive body z-axis direction. Considering the presence of a low-level attitude controller which controls the roll, pitch and yaw of the vehicle, the dynamics of a multirotor UAV can be modeled as [18], [19]

$$m_i\ddot{x}_i = \tau_i + b_{L,i} + b_{W,i} - m_i g \tag{1}$$

where $x_i(t) \in \mathbb{R}^3$ is the position of UAV i in the inertial North-East-Down (NED) frame, and m_i its mass. The UAV is affected by a gravitational force $m_i g$, $g \in \mathbb{R}^3$. The suspended load affects multirotor i with an unknown force $b_{L,i}(t) \in \mathbb{R}^3$. Further, the vehicle is affected by a slowly varying wind force $b_{W,i}(t) \in \mathbb{R}^3$. The force vector $\tau_i(t) \in \mathbb{R}^3$ is a virtual control input to a low-level attitude controller, which can be translated to a desired roll and pitch angle as described in [18]. For the experimental trials described later in this paper, we utilize the algorithm provided by the Ardupilot [20] autopilot software, which computes the necessary roll (ϕ_d) and pitch (θ_d) angles from the body-aligned forces F_x^b, F_y^b as

$$\theta_d = \arctan\frac{-F_x^b}{m_i g} \tag{2}$$

$$\phi_d = \arctan\frac{F_y^b \cos\theta_d}{m_i g} \tag{3}$$

which is valid for low vertical accelerations. The body-aligned control forces are calculated from the current UAV yaw angle and the desired NED virtual control force τ_i.

Let the load be suspended under N multirotors as depicted in Figure 1. The suspended load dynamics are governed by

$$m_L\ddot{x}_L = b_{L,L} - m_L g \tag{4}$$

where $x_L(t) \in \mathbb{R}^3$ and m_L is the position of the load in the NED-frame and the mass of the load, respectively. $b_{L,L}(t) \in \mathbb{R}^3$ is the force acting on the suspended load to lift it, which is equal to $\sum_{i=1}^{N} b_{L,i}$.

For notational simplicity, we introduce the concatenated position vector x as

$$x := [x_1^\top, \cdots, x_n^\top]^\top \in \mathbb{R}^{3N}$$

When connecting multiple UAVs to the same payload, the constraint forces of b_i^L is a highly dynamic function from the multi-body interactions of all UAVs in the system. For simulation purposes, the forces from the constraints can be calculated in different ways. In this article, we utilize the Udwadia-Kalaba equation [21] to explicitly calculate the forces of constraints on each vehicle. The constraint forces are a function of the accelerations of all involved bodies, and are thus most suited for simulation purposes. The control strategy presented in Section III assumes these forces are unknown, so they don't need to be measured or estimated explicitly. This technique has previously been applied to similar systems in [22], [23], in which details on the derivations can be found.

Consider the wire i connecting UAV i with the load. The taut wire imposes a constraint on the two bodies, of the form

$$g_i = ||\mathbf{L}_i||^2 - l_i^2 = 0 \tag{5}$$

where l_i is the nominal length of the wire, and $\mathbf{L}_i := x_i - x_L$. (5) can be double-differentiated, and put on the standard form

$$\mathbf{A}_i(x, \dot{x}, x_L, \dot{x}_L)\ddot{x} = \mathbf{b}_i(x, \dot{x}, x_L, \dot{x}_L) \tag{6}$$

Then, the total constraint force b_L from all the wires can be calculated by

$$b_L = \mathcal{M}^{1/2}(\mathbf{A}\mathcal{M}^{-1/2})^+(\mathbf{b} - \mathbf{A}\ddot{x}) \tag{7}$$

where $\mathcal{M}$, $\mathbf{A}$ and $\mathbf{b}$ are concatenations of $m_i, \mathbf{A}_i$ and $\mathbf{b}_i$, respectively and as depicted below, and $(\cdot)^+$ denotes the Moore-Penrose pseudo inverse. The structure of the matrices are

$$\mathcal{M} = \begin{bmatrix} m_1 I_3 & 0 & \cdots & 0 \\ 0 & m_2 I_3 & \cdots & 0 \\ 0 & 0 & \ddots & 0 \\ 0 & 0 & 0 & m_N I_3 \end{bmatrix} \in \mathbb{R}^{3N\times 3N} \tag{8}$$

$$\mathbf{A} = \begin{bmatrix} \mathbf{A}_1 \\ \mathbf{A}_2 \\ \vdots \\ \mathbf{A}_N \end{bmatrix} \in \mathbb{R}^{3N\times 3N}, \quad \mathbf{b} = \begin{bmatrix} \mathbf{b}_1 \\ \mathbf{b}_2 \\ \vdots \\ \mathbf{b}_N \end{bmatrix} \in \mathbb{R}^{3N} \tag{9}$$

For control synthesis purposes, we consider the the disturbances $b_{L,}$ and $b_{W,i}$ on each multirotor UAV unknown, and re-write (1) as

$$m_i\ddot{x}_i = \tau_i - m_i g + \theta_i \tag{10}$$

where the wind and load drag force is lumped together in θ_i:

$$\theta_i := b_{L,i} + b_{W,i} \tag{11}$$

Note that in the following adaptive design, the disturbance force from the load is considered a constant bias. However, as stated above, the magnitude of the disturbance changes as a function of the acceleration of the involved multirotors.

Nonetheless, the assumption is valid for constant velocities, and only minor deviations occur when accelerating.

We assume the UAVs are communicating with each other, where the communication topology is represented by a graph's incidence matrix M [24]. As an example for three UAVs communicating with each other, we have the following incidence matrix M:

$$M = \begin{bmatrix} 1 & 0 & -1 \\ -1 & 1 & 0 \\ 0 & -1 & 1 \end{bmatrix}$$

For other numbers of UAVs N, the incidence matrix is constructed accordingly. We also define the matrix $D := M \otimes I_3 \in \mathbb{R}^{3N\times 3N}$, where $\cdot \otimes \cdot$ is the Kronecker product, which is used in the next sections to map the effect of the communication topology to the position vector in $\mathbb{R}^3$.

III. Control Strategy

The goal is to design a *decentralized* control structure for each UAV that utilizes relative position and velocity from their neighbors to converge to a desired formation moving with a common mission velocity $v(t) \in \mathbb{R}^3$ and to correct for the unknown disturbances from the wind and the suspended load. We follow the *passivity based approach* in [24], which defines the following desired group behaviors

A1) Each agent achieves in the limit the common mission velocity vector as

$$\lim_{t\to\infty} |\dot{x}_i - v(t)| = 0, \quad i = 1, \cdots, N \tag{12}$$

A2) If vehicles i and j are connected by link k, then the difference variable z_k

$$z_k := \sum_{l=1}^{N} M_{lk} x_l = \begin{cases} x_i - x_j & \text{if } k \in \mathscr{L}_i^+ \\ x_j - x_i & \text{if } k \in \mathscr{L}_i^- \end{cases} \tag{13}$$

converges asymptotically to z_k^d defined below, where $\mathscr{L}_i^+ (\mathscr{L}_i^-)$ represents the set of communication links on the positive (negative) end, respectively.

Let

$$z := [z_1^\top, \cdots, z_N^\top]^\top \in \mathbb{R}^{3N}$$

then, we can re-write (13) as

$$z = D^\top x. \tag{14}$$

where D is defined as in Section II. Now let $x^d \in \mathbb{R}^{3N}$ be a constant vector describing the desired formation of the UAVs (an example is given in Section IV), and define

$$z^d = D^\top x^d \tag{15}$$

A. Internal Feedback Control

First, we design an *internal feedback* controller. Let the control input τ_i be defined as below, which is designed based on a passivity-based approach which will become apparent later:

$$\begin{aligned} \tau_i = &- k_i(\dot{x}_i - v(t) - \Gamma_i u_i) \\ &+ m_i(\dot{v}(t) + \Gamma_i \dot{u}_i) \\ &+ m_i g + u_i - \hat{\theta}_i \end{aligned} \tag{16}$$

where $\Gamma_i = \Gamma_i^\top > 0 \in \mathbb{R}^{3\times 3}$ is a tuning matrix, $k_i > 0$ is a scalar gain, u_i is an external signal from the formation controller to be specified, and $\hat{\theta}_i$ is our estimate of θ_i, governed by the update-law

$$\dot{\hat{\theta}}_i = \Lambda_i \xi_i \tag{17}$$

where $\Lambda_i = \Lambda_i^\top > 0 \in \mathbb{R}^{3\times 3}$ and

$$\xi_i = \dot{x}_i - v(t) - \Gamma_i u_i \tag{18}$$

With the control input (16) and the error-variable ξ_i defined in (18) above, the UAV dynamics (10) forms a subsystem $\mathscr{H}_i$ with inputs $-\tilde{\theta}_i + u_i$ and output y_i:

$$\dot{x}_i = y_i + v(t) + \Gamma_i u_i \tag{19}$$

$$\mathscr{H}_i : \begin{cases} m_i \dot{\xi}_i = -k_i \xi_i + u_i - \tilde{\theta}_i \\ y_i = \xi_i \end{cases} \tag{20}$$

where

$$\tilde{\theta}_i := \hat{\theta}_i - \theta_i. \tag{21}$$

B. Formation Control

Next, the external control signal u_i is designed to stabilize the formation. Consider

$$u_i = -\sum_{k=1}^{N} M_{ik} \Psi_k(z_k) \tag{22}$$

where

$$\Psi_k(z_k) = \kappa_k(z_k - z_k^d) \tag{23}$$

where $\kappa_k = \kappa_k^\top > 0 \in \mathbb{R}^{3\times 3}$ is a block diagonal matrix of gains. $\mathcal{K}$ represents the diagonal concatenation matrix of all κ_k. To clarify notation, let $\tilde{z}_k$, and its corresponding stacked vector $\tilde{z}$ be defined as

$$\tilde{z}_k := z_k - z_k^d, \quad \tilde{z} := z - z^d \tag{24}$$

u can now be re-written as

$$u = -D\mathcal{K}\tilde{z}. \tag{25}$$

C. Stability Analysis

The dynamics of the link errors $\tilde{z}$, velocity errors ξ and bias estimate error $\tilde{\theta}$ is now a set of interconnected subsystems, as illustrated in Figure 2. The stability properties of the proposed control structure is given in the next theorem, which is an adaptation of [24, Th. 6.2].

Theorem 1. *Consider N multirotors carrying a suspended load, modeled as* (10)*, with the control input* (16) *and $\hat{\theta}_i$ updated as in* (17)*. Then, the origin of $(\tilde{z}, \xi, \tilde{\theta})$ is globally asymptotically stable, which means that $|\dot{x}_i - v(t)| \to 0$, $|z_k(t) - z_k^d| \to 0$ and $|\dot{\hat{\theta}}_k(t) - \theta_k| \to 0$.*

Proof. In the following proof, we utilize passivity as a tool for stability analysis and analyze the subsystems sequentially, as in [24]

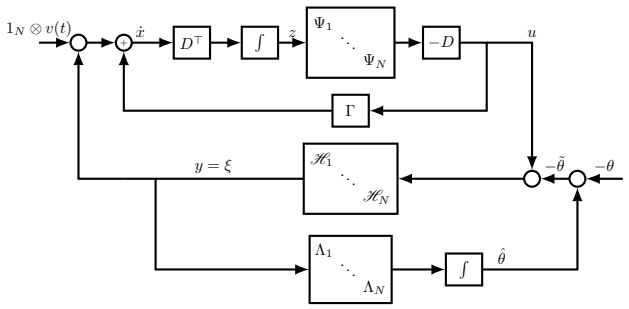

Fig. 2. System interconnection with unknown disturbances θ acting on the system.

i) Feedforward path: We first prove passivity from y to $-u$. Let V_f be a storage function:

$$V_f(\tilde{z}) = \frac{1}{2}\sum_{k=1}^{N} \tilde{z}_k^\top \kappa_k \tilde{z}_k \tag{26}$$

whose derivative along the solutions of

$$\dot{\tilde{z}} = D^\top \dot{x} \tag{27}$$

is

$$\begin{aligned} \dot{V}_f(\tilde{z}) &= \tilde{z}^\top \boldsymbol{\kappa} D^\top (\dot{x}) && (28)\\ &= \tilde{z}^\top \boldsymbol{\kappa} D^\top (y + 1_N \otimes v(t) + \Gamma u) && (29)\\ &= \tilde{z}^\top \boldsymbol{\kappa} D^\top (y + \Gamma u) && (30)\\ &= -u^\top \Gamma u - u^\top y && (31) \end{aligned}$$

which shows strict passivity from y to $-u$, where we have used (25) and $D^\top(1_N \otimes v(t)) \equiv 0$.

ii) Feedback path: Next, we analyse the $\mathscr{H}_i$ subsystems, and show that the interconnection with the formation controller through u_i renders these two subsystems passive from the bias estimate error $\tilde{\theta}$ to y. Let a storage function for $\mathscr{H}_i$ be

$$V_b(\xi) = \sum_{i=1}^{N} \frac{1}{2} m_i \xi_i^\top \xi_i \tag{32}$$

whose derivative evaluates to

$$\begin{aligned} \dot{V}_b(\xi) &= \sum_{i=1}^{N} (-k_i \xi_i^\top \xi_i - \xi_i^\top \tilde{\theta}_i) + u^\top y && (33)\\ &= -\xi^\top K \xi + u^\top y - \tilde{\theta}^\top y && (34) \end{aligned}$$

where $K = (k_i \otimes I_3) \otimes I_N$ and $y_i = \xi_i$ as in (18).

iii) Finally, let $V(\tilde{z}, \xi, \tilde{\theta})$ be a Lyapunov function, defined by

$$V(\tilde{z}, \xi, \tilde{\theta}) = V_f(\tilde{z}) + V_b(\xi) + \frac{1}{2}\sum_{N} \tilde{\theta}_i^\top \Lambda_i^{-1} \tilde{\theta}_i \tag{35}$$

which satisfies $V(\tilde{z}, \xi, \tilde{\theta}) > 0$ for $(\tilde{z}, \xi, \tilde{\theta}) \neq 0$ and $V(0) = 0$, whose derivative along the solutions of the system are

$$\dot{V}(\tilde{z}, \xi, \tilde{\theta}) = -\tilde{z}^\top \boldsymbol{\kappa} D^\top \Gamma D \boldsymbol{\kappa} \tilde{z} - \xi^\top K \xi \leq 0 \tag{36}$$

where the last term in (34) is eliminated by the last term in (35) after substituting of the update-law for $\dot{\hat{\theta}}_i$ given in (17).

$\dot{V}(\tilde{z}, \xi, \tilde{\theta})$ is negative semi-definite since $D^\top \Gamma D \geq 0$, and implies stability of the origin and boundedness of $(\tilde{z}, \xi, \tilde{\theta})$. Note that $\dot{V} = 0$ when $D\boldsymbol{\kappa}\tilde{z} = 0$, that is when $\boldsymbol{\kappa}\tilde{z}$ is in the null space of D. By construction, $\tilde{z}$ is in the range space of $D^\top$. Thus, $\tilde{z}$ is orthogonal to $\boldsymbol{\kappa}\tilde{z}$ since the range space of $D^\top$ is orthogonal to the null space of D, and $\tilde{z}^\top \boldsymbol{\kappa} \tilde{z} = 0$ which implies $\tilde{z} = 0$. Further, from (25) and (20), we have $\tilde{\theta} = 0$. We then apply the Invariance principle, and since $V(\tilde{z}, \xi, \tilde{\theta})$ is radially unbounded and satisfies $V(0, 0, 0) = 0$, we have shown global asymptotic stability of $(\tilde{z}, \xi, \tilde{\theta})$.

□

In the next section, a numerical simulation study illustrates the proposed controller.

IV. Simulation Study

As an example, consider the configuration with $N = 3$ UAVs carrying the suspended load. Let each UAV have a mass $m = 2$ kg, and the load have mass $m_L = 3$ kg connected with wires of length $l_i = 2$ m. In addition to the reaction force from the load, the UAVs are also affected by a constant wind v_w in the NED-x-direction with a magnitude of 4 m/s. To calculate the resulting disturbance force b_i^w, we use the relationship $b_i^w = dv_w$, using

For $N = 3$, a fully connected graph between all UAVs consists of three links and the resulting control incidence matrix M is given by

$$M = \begin{bmatrix} 1 & 0 & -1 \\ -1 & 1 & 0 \\ 0 & -1 & 1 \end{bmatrix}. \tag{37}$$

Suppose we want the three UAVs to form a triangle with each side having length $\Delta \in \mathbb{R}$. We let $x_i^d \in \mathbb{R}^3$ for $i = 1, \ldots, N$ represent the desired positions of the UAVs and assume that

$$x_1^d = \begin{bmatrix} 0 \\ 0 \\ 0 \end{bmatrix}.$$

Then a set of possible desired positions of the UAVs are described by

$$x_2^d = \begin{bmatrix} \Delta \\ 0 \\ 0 \end{bmatrix} \quad \text{and} \quad x_3^d = \begin{bmatrix} \Delta/2 \\ \Delta\sqrt{3}/2 \\ 0 \end{bmatrix}.$$

The desired relative positions z^d are then given by

$$z^d = (M \otimes I_3)^\top \begin{bmatrix} x_1^d \\ x_2^d \\ x_3^d \end{bmatrix}. \tag{38}$$

We let the initial positions $x_i^0 = x_i(t = 0)$ of the UAVs be

$$x_1^0 = \begin{bmatrix} 0 \\ 0 \\ 0 \end{bmatrix}, \quad x_2^0 = \begin{bmatrix} 3 \\ 0 \\ 0 \end{bmatrix}, \quad x_3^0 = \begin{bmatrix} 0 \\ 1 \\ 0 \end{bmatrix},$$

and the desired formation be given by (38) with $\Delta = 2$. We also include a constant desired mission velocity, that tends the multirotors to carry the load at 1 m/s in the positive x-direction.

A. Results

As can be seen in Figure 3 and Figure 4b, the multirotors tends towards the desired formation. We see that the links converge to their actual desired values in Figure 5 despite the disturbances from the unknown load and the constant wind force, due to the convergence of the bias compensation term θ_i as seen in Figure 6. As the vehicles approach their final relative positions, the actual force on each UAV from the suspended load is changing as can be seen in the beginning of Figure 4b and Figure 6. However, the terms converge when the UAVs reach their formations. Note that the different end values in Figure 6 is due to the effect of the combined disturbance from the wind and suspended load, which is different for each UAV.

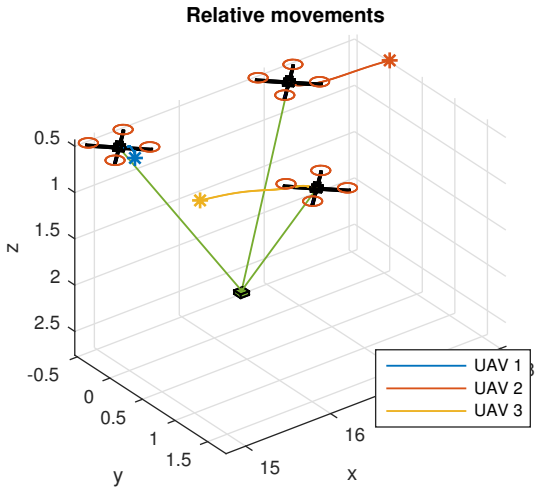

Fig. 3. Final position of the three UAVs and the suspended load. The figure shows the relative movements between the vehicles, with the mean position subtracted. For each UAV an asterix denotes the initial position.

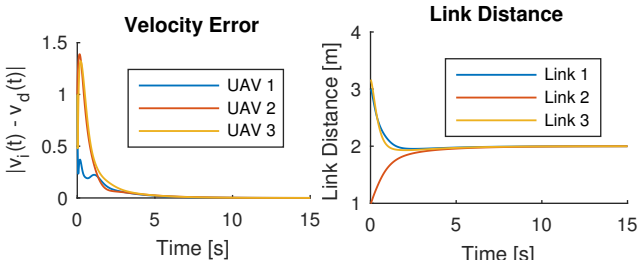

(a) The velocity error relative to the desired velocity v^d for each UAV. (b) Distance between each UAV.

Fig. 4. Velocity error and link distance.

V. Experimental Validation

To further validate the proposed controller, experimental trials with three multirotors carrying a suspended load was conducted. The UAV platform is a hexacopter with weight $m_c = 2.3$ kg, equipped with the *Pixhawk* [25] autopilot system running Ardupilot [20] software. This autopilot handles sensor fusion from its internal IMU and GNSS systems, as well as low level attitude control. It receives attitude and thrust setpoints from an on-board Linux computer, a Beaglebone Black, which contains the custom controller described in this work. The

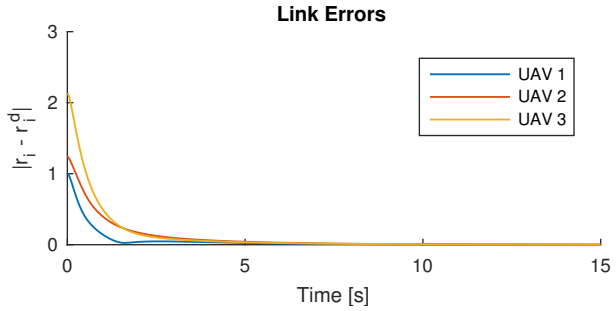

Fig. 5. The link error between the UAVs.

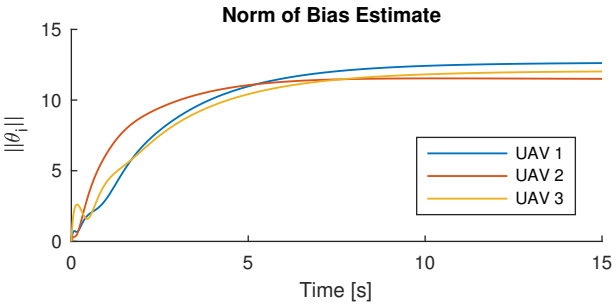

Fig. 6. The norm of the integral term θ_i for each UAV. The values converge to the sum of disturbance of the suspended load and wind force for each UAV.

Beaglebone is a 1 GHz single-board ARM computer, running the LSTS toolchain [26]. This toolchain consists of a Linux distribution (Glued), a ground station segment (Neptus) and a vehicle software stack (DUNE). More details can also be found in [27]. All implementations for the experimental validation are implemented in DUNE using C++.

The desired relative position was given by the initial position on the ground, which was set to an equal-sided triangle, with sides of 5 m. The control software was implemented such that a single pilot can perform coordinated takeoff, and use a remote controller to set reference velocities and accelerations during the test. The communication links are organized as in (37). An image of the three multirotors successfully transporting a suspended load is given in Figure 1.

It should be noted that as it is not possible to attach the load at the exact centre of gravity of the UAVs, resulting in a slight moment-arm from the load on the UAV body. The magnitude of this disturbance is also dependent on the total configuration of the system, including number of UAVs used and their relative distances. In the proposed control structure, this disturbance is counteracted by the integral effect of the low-level attitude controller, such as the one implemented in the autopilot. As this moment arm adds extra strain on some of the UAV motors, care should be taken to ensure that the UAV motors are not saturated by this effect, which would make the UAV incapable of maintaining maneuverability. To test these conditions given the set of system parameters, flight characteristics were carefully monitored during preliminary experiments by gradually increasing the weight of the suspended load. Alternatively, simulation studies could be conducted to ensure the saturation is not reached. In the configuration described in this section, the autopilot successfully counter-acted these effects.

Two main tests were conducted. In the first, a lighter load

of approx. 1 kg was used, and in the second a heavier load of approx. 2.2 kg. Figure 1 shows the UAVs with the light load. In general, choosing the configuration of UAVs to carry a specified load is a matter of design tradeoffs involving, among others, operation complexity, UAV carrying capacity and necessary flight-time. For multirotor UAVs, a rule of thumb is to let the total UAV take-off weight be approximately 50% of its maximum flight weight to leave sufficient room for high maneuverability. This number can be higher if less maneuverability is required. As noted above, these criterions can be verified in simulations or tests on the UAV platform under controlled conditions. In our case, our 2.2 kg UAVs can carry up to 1 kg additional payload while still maintaining sufficient maneuverability and flight-time. For the heavy weight of 2.2 kg, this would leave each multirotor carry approximately 0.73 kg, which is within these bounds. Note however that two multirotors alone would not have been able to carry this weight.

In Figures 7–9 a summary of the two experiments are illustrated. In each figure, the upper plot shows the sum of link-error norms $\sum |\tilde{z}_k|$, the middle shows the norm of acceleration setpoint $|\dot{v}^d(t)|$, and the lower shows the norm of the bias term for all multirotors. In both cases the controllers are able to maintain a relatively close formation, but during heavy accelerations a somewhat larger error is seen. However, it is quickly recovered once the acceleration-phase is over.

Due to heavy winds on the test-day (estimated 4-6 m/s from the right to the left as shown in Figure 1), the rightmost multirotor (UAV 2) has an increased load due to air drag on the suspended load. This is also seen by the lower plots in Figures 7–9. As can also be seen, the bias term saturates at a maximum level, which was set to a too low value during the experiments.

TABLE I
MEAN LINK ERROR OVER THE TWO EXPERIMENTS.

Mean Link Error [m]	**Light load**	**Heavy load**
Link 1	0.38	0.57
Link 2	0.37	0.34
Link 3	0.16	0.46

Nonetheless, as can be seen in Figure 11, the link errors remain relatively small during the entire experiment. A summary of the *mean link errors* are provided in Table I. It is seen that for the light experiment, the mean errors are below 0.4 m, while for the heavier load they are slightly higher. A video of the experimental trial is available online: https://youtu.be/seqpCEx3mY0. The video shows the raw footage from the experiment, starting with the simultaneous takeoff of all three multirotor UAVs. After a settling time, the UAV operator generates the common velocity reference signals to guide the formation back and forth over the field. Next, the light load (1 kg) is substituted for the heavier (2.2 kg) load, and the procedure is repeated.

Further, the reference velocity and velocity error are shown in Figure 8 and Figure 10 for the two experiments. For both figures, the top part depicts the reference speed as set on-site by the UAV operator using a remote controller, compared to the average speed of all UAVs. The average is taken for figure clarity. The lower part shows the average of the norm of the velocity error. As can be seen, after the bias estimation starts to converge, the velocity error is relatively small and the UAVs track the reference velocity even with a very dynamic reference trajectory.

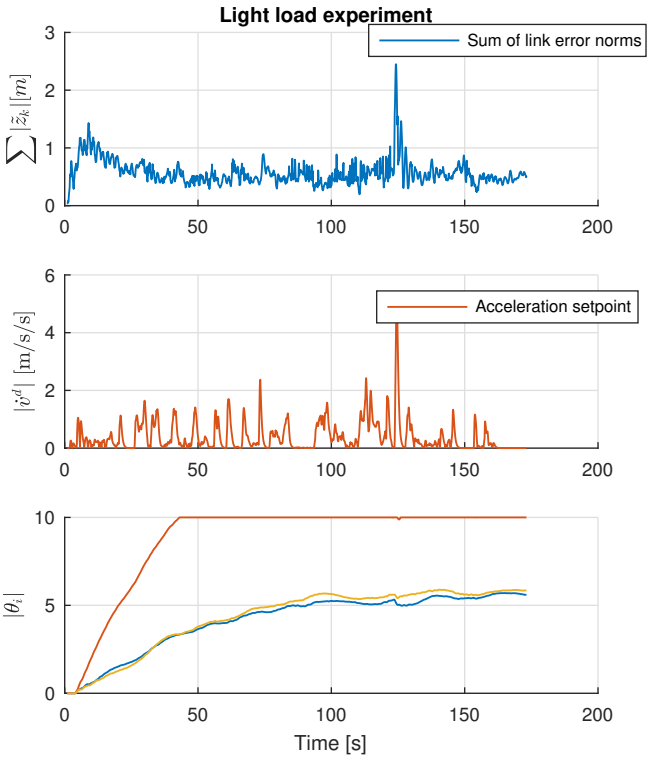

Fig. 7. Summary of the first (light) experiment. The lower plots shows the norm of bias estimation for the first (blue), second (red) and third (yellow) multirotor UAV.

VI. Conclusion

In this article, we have developed a cooperative control strategy for a group of multirotors carrying a suspended load. After an introduction to the system dynamics and modeling, a mathematical stability proof using Lyapunov theory of the proposed control solution is presented, following a passivity-based approach. To further validate the proposed design, numerical simulation and results from experimental trials are presented. The results show convergence to the desired relative formation of the interconnected UAVs in the presence of unknown wind and suspended load conditions.

References

[1] M. Bernard and K. Kondak, "Generic slung load transportation system using small size helicopters," *Proceedings of the 2009 IEEE International Conference on Robotics and Automation*, pp. 3258–3264, 2009.

[2] K. Sreenath, T. Lee, and V. Kumar, "Geometric control and differential flatness of a quadrotor UAV with a cable-suspended load," in *Proceedings of the IEEE Conference on Decision and Control*, 2013, pp. 2269–2274.

[3] Nimbus.unl.edu, "Co-Aerial-Ecologist: Robotic Water Sampling and Sensing in the Wild," 2017. [Online]. Available: https://nimbus.unl.edu/projects/co-aerial-ecologist-robotic-water-sampling-and-sensing-in-the-wild/

[4] Theverge.com, "This drone can detect and detonate land mines," 2016. [Online]. Available: http://www.theverge.com/2016/7/19/12222104/landmine-detecting-drone-mine-kafon-drone

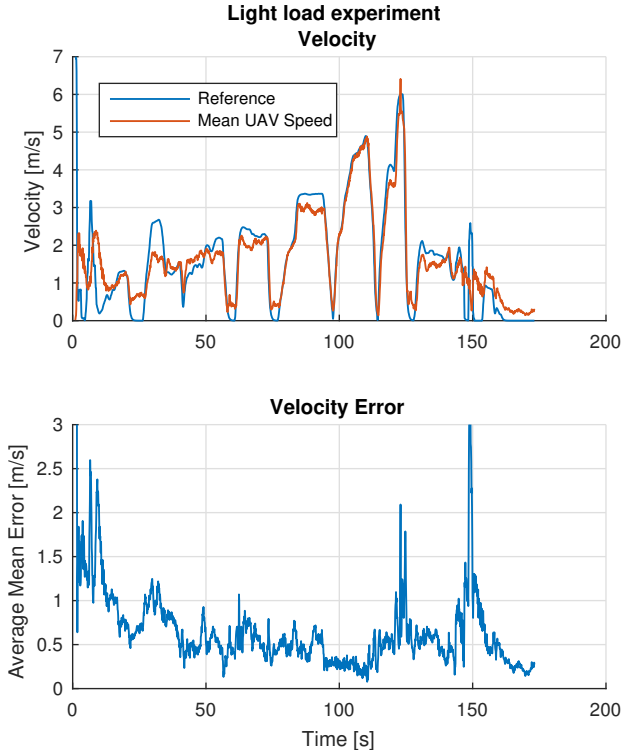

Fig. 8. Top: The average norm of velocity for each UAV relative to the reference. Bottom: Average norm of the velocity error for each UAV.

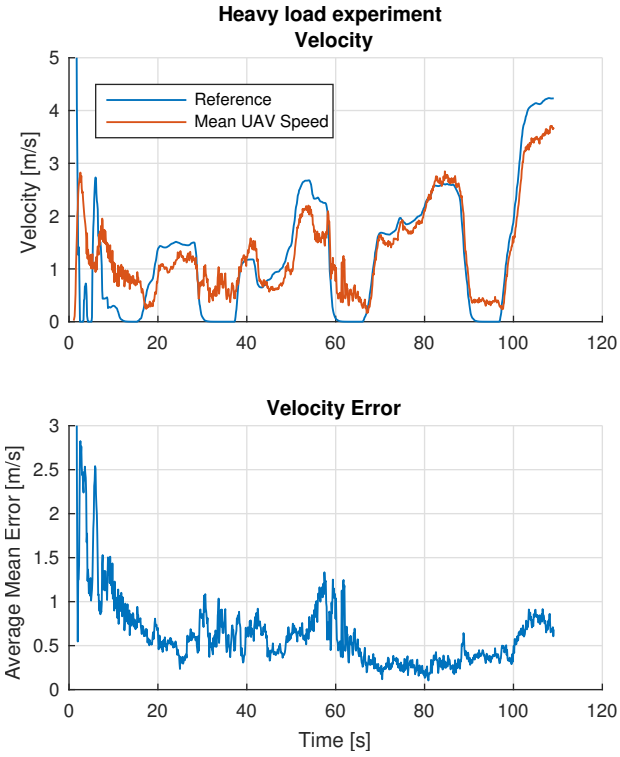

Fig. 10. Top: The average norm of velocity for each UAV relative to the reference during the heavy load experiment. Bottom: Average norm of the velocity error for each UAV for the heavy load experiment.

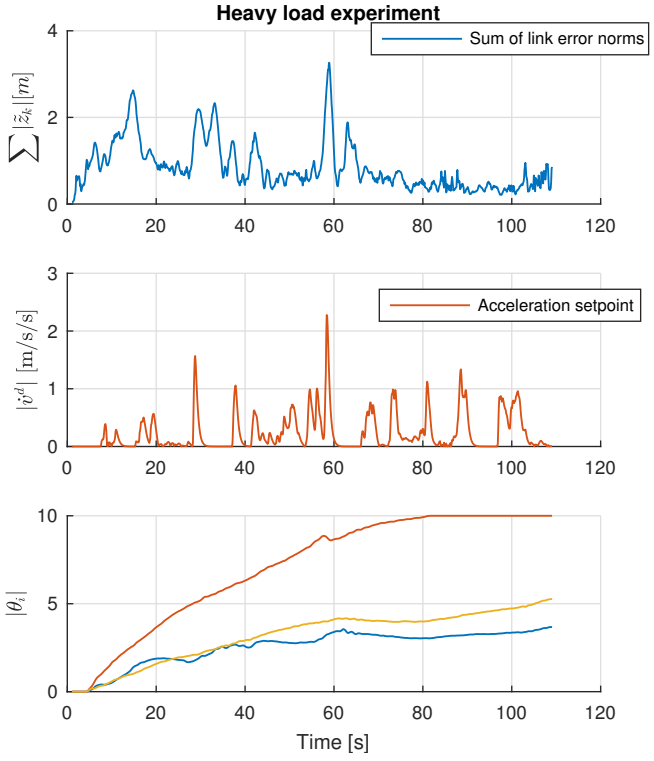

Fig. 9. Summary of the second (heavy) experiment. The lower plots shows the norm of bias estimation for the first (blue), second (red) and third (yellow) multirotor UAV.

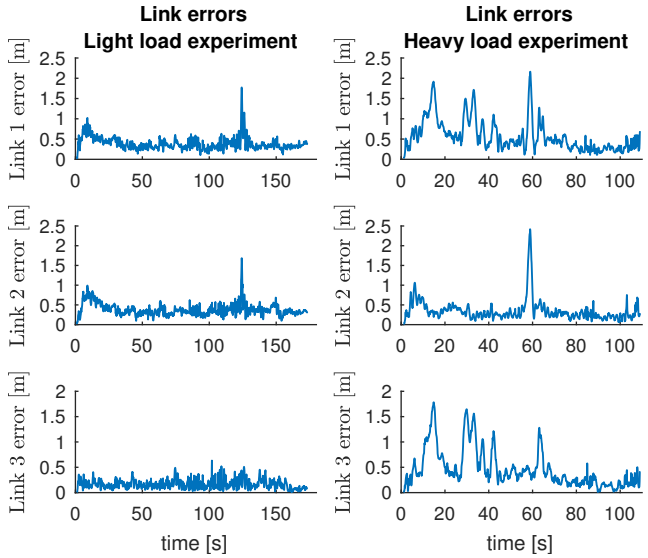

(a) Norm of the link errors for links 1-3 for the experiment with the lighter load.

(b) Norm of the link errors for links 1-3 for the experiment with the heavier load.

Fig. 11. The position error (link error) between the multirotors for the light load (a) and heavy load (b) experiment.

[5] K. Klausen, T. I. Fossen, and T. A. Johansen, "Autonomous Recovery of a Fixed-Wing UAV Using a Net Suspended by Two Multirotor UAVs," *Journal of Field Robotics (to appear)*, 2018.
[6] Cnbc.com, "Dominos Pizza Drone Delivery," 2016.
[7] Amazon, "Amazon.com," 2016. [Online]. Available: http://www.amazon.com/b?node=8037720011
[8] Zipline.com, "Zipline - Lifesaving Deliveries," 2017. [Online]. Available: http://flyzipline.com/
[9] I. Maza, K. Kondak, M. Bernard, and A. Ollero, "Multi-UAV Cooperation and Control for Load Transportation and Deployment," *Journal of Intelligent and Robotic Systems*, vol. 57, no. 1-4, pp. 417–449, aug 2009.
[10] N. Michael, J. Fink, and V. Kumar, "Cooperative manipulation and transportation with aerial robots," *Autonomous Robots*, vol. 30, no. 1, pp. 73–86, sep 2010.
[11] J. Fink, N. Michael, S. Kim, and V. Kumar, "Planning and control for cooperative manipulation and transportation with aerial robots," *The International Journal of Robotics Research*, vol. 30, no. 3, sep 2010.
[12] T. Lee, K. Sreenath, and V. Kumar, "Geometric Control of Cooperating Multiple Quadrotor UAVs with a Suspended Payload," in *Proceedings of the 52nd IEEE Conference on Decision and Control*, 2013, pp. 5510–5515.
[13] F. A. Goodarzi and T. Lee, "Stabilization of a Rigid Body Payload with Multiple Cooperative Quadrotors," *Journal of Dynamic Systems, Measurement, and Control*, vol. 138, no. 12, 2016.
[14] K. Klausen, T. I. Fossen, T. A. Johansen, and A. P. Aguiar, "Cooperative path-following for multirotor UAVs with a suspended payload," *Proceedings of the 2015 IEEE Conference on Control Applications (CCA)*, pp. 1354–1360, 2015.
[15] G. Tartaglione, E. D'Amato, M. Ariola, P. S. Rossi, and T. A. Johansen, "Model predictive control for a multi-body slung-load system," *Robotics and Autonomous Systems*, vol. 92, pp. 1–11, 2017.
[16] C. Meissen, K. Klausen, M. Arcak, T. I. Fossen, and A. Packard, "Passivity-based Formation Control for UAVs with a Suspended Load," in *Proceedings of the IFAC World Congress*, 2017.
[17] H. Bai, M. Arcak, and J. T. Wen, "Group Coordination when the Reference Velocity is Available Only to the Leader: An Adaptive Design," *2007 American Control Conference*, no. 3, pp. 5400–5405, jul 2007. [Online]. Available: http://ieeexplore.ieee.org/lpdocs/epic03/wrapper.htm?arnumber=4282711
[18] R. Mahony, V. Kumar, and P. Corke, "Modeling, Estimation, and Control of Quadrotor," *IEEE Robotics and Automation Magazine*, vol. 19, no. 3, pp. 20–32, sep 2012.
[19] K. Klausen, T. I. Fossen, and T. A. Johansen, "Nonlinear Control with Swing Damping of a Multirotor UAV with Suspended Load," *Journal of Intelligent & Robotic Systems*, 2017.
[20] Ardupilot.com, "Ardupilot - Open source autopilot," 2016. [Online]. Available: http://ardupilot.com
[21] F. E. Udwadia and R. E. Kalaba, *Analytical Dynamics: A New Approach*, 1st ed. Cambridge University Press1, 1996.
[22] M. Bisgaard, J. D. Bendtsen, and A. L. Cour-Harbo, "Modeling of Generic Slung Load System," *Journal of Guidance, Control, and Dynamics*, vol. 32, no. 2, pp. 573–585, mar 2009.
[23] K. Klausen, T. I. Fossen, and T. A. Johansen, "Suspended Load Motion Control using Multicopters," in *Proceedings of the Mediterranean Conference of Control and Automation (MED)*. Palermo: IEEE, 2014, pp. 1371–1376.
[24] H. Bai, M. Arcak, and J. T. Wen, *Cooperative control design: A systematic, passivity-based approach*. Springer-Verlag New York, 2011.
[25] Pixhawk.ethz.ch, "PX4 Pixhawk," 2016. [Online]. Available: https://pixhawk.ethz.ch/
[26] J. Pinto, P. S. Dias, R. Martins, J. Fortuna, E. Marques, and J. Sousa, "The LSTS toolchain for networked vehicle systems," in *Proceedings of the MTS/IEEE OCEANS*. Bergen: MTS/IEEE, 2013.
[27] A. Zolich, T. A. Johansen, K. Cisek, and K. Klausen, "Unmanned Aerial System Architecture for Maritime Missions. Design & Hardware Description," in *Workshop on Research, Education and Development of Unmanned Aerial Systems (RED-UAS)*. IEEE, 2015.